

Numerical simulation of the plasma generated by the interaction high-current electron beam with *Al* target

D. Levko,¹ Ya. E. Krasik,¹ W. An,² and G. Mueller²

¹*Physics Department, Technion, 32000 Haifa, Israel*

²*Karlsruhe Institute of Technology, P.O. Box 3640, 76021 Karlsruhe, Germany*

(Received 17 February 2013; accepted 15 March 2013; published online 28 March 2013)

The results of one dimensional particle-in-cell simulations of the dynamics of plasma generated during the interaction of a high-energy (≤ 200 keV) and high-current (≤ 15 A/cm²) electron beam with an aluminum target are presented. The generated target plasma is low-ionized and characterized by non-Maxwellian electron energy distribution. The density and electron temperature of the plasma, which expands toward the anode at a typical velocity of $\sim 10^5$ cm/s, does not exceed 4×10^{14} cm⁻³ and 1 eV, respectively, which is in satisfactory agreement with the experimental results presented in W. An *et al.*, *J. Appl. Phys.* **110**, 093304 (2011). The results of the simulations showed also acceleration of the ions from the target plasma toward the anode by the potential of the non-compensated space charge of the electron beam. The typical velocity of these energetic ions is $\sim 10^8$ cm/s and depends on the electron current density and energy. These ions partially compensate the space charge of the electron beam, which leads to a decrease in the depth of the potential well. © 2013 American Institute of Physics.
[\[http://dx.doi.org/10.1063/1.4798586\]](http://dx.doi.org/10.1063/1.4798586)

I. INTRODUCTION

Today, intense experimental and theoretical research studies¹⁻⁶ are being devoted to the modification of metal surface properties using pulsed (10^{-7} – 10^{-4} s) high-current (1–100 A/cm²) electron and ion beams with an energy up to several hundreds of keV. The interaction of such beams with a target is accompanied by different phenomena, which include extremely fast heating and cooling of the surface layer, generation of a large pressure gradient, and different phase transitions (solid state – liquid – vapor – plasma) of the target material. As a result of this interaction, one can obtain significant improvement in various properties (hardness, corrosion, elasticity, etc.) of the target surface layer with a depth up to several tens of μ m.

One of the interesting and unavoidable features of this beam-target interaction is the generation of plasma in the vicinity of the metal target, which can influence significantly the processes of surface property modification. In the case of high-current electron beams, this plasma is formed by the electron impact ionization of adsorbed gas monolayers and metal atoms evaporated from the target heated by the high-energy electron beam. The plasma ions can propagate in the direction opposite to that of the electron beam transportation, leading to neutralization of the electron beam space charge and, respectively, changing the properties of the beam transport. In addition, when a transparent anode is used, these ions can significantly change the impedance of the diode where electron beam generation occurs.

The properties of target plasma are not yet well understood and require both experimental and theoretical studies. Analytical modeling of plasma formation on the target surface as a result of interaction with an electron beam having a duration $> 10^{-5}$ s, current density of ~ 10 A/cm², and

electron energy of $\sim 10^5$ eV was conducted in Ref. 6. It was shown that the time necessary for plasma formation to occur depends on the current density of the beam, and that the ion flux, which is generated in the vicinity of the target, influences significantly the energy of the electron beam and neutralizes its space charge. In addition, it was shown that the target plasma is expanded into the beam drift region, with the velocity increasing in time. However, this modeling does not consider self-consistently the processes related to the plasma formation and electric field development in the drift space and in the vicinity of the target.

Recent experimental studies⁷ carried out in the Karlsruhe Institute of Technology using high-current electron beams having a duration up to 200 μ s and typical electron energy $\varepsilon_b \sim 100$ keV, and electron current density on the target $j_b \sim 10$ A/cm² that were generated by pulsed electron beam facility GESA I and GESA II facilities^{3,4} allowed some basic properties of the plasma generated in the vicinity of the different metal targets to be defined. Namely, it was shown that, at a time delay of ≥ 40 μ s with respect to the beginning of the interaction of the electron beam with a target, one obtains intense evaporation of neutrals from the target surface with a typical velocity of $\sim 2 \times 10^5$ cm/s and rate of evaporation of 10^{24} particle/(cm²·s), and that the density and electron temperature of the generated plasma reaches $n_e \leq 4 \times 10^{14}$ cm⁻³ and $T_e \sim 0.5$ eV, respectively.

In this paper, the results of one-dimensional particle-in-cell (1D PIC) simulations of the dynamics of plasma generated during the interaction between a high-energy electron beam and the *Al* vapors formed at the surface of an *Al* target are presented. It is shown that the plasma is non-Maxwellian, with a typical plasma density of $\leq 4 \cdot 10^{14}$ cm⁻³; the average energy of the plasma electrons is ≤ 1 eV; and the velocity of the plasma front propagation toward the anode is $\sim 10^6$ cm/s.

II. NUMERICAL MODEL

In the model, a magnetized rigid electron beam generated in the vacuum diode and transported towards the target in the guiding magnetic field (see Fig. 1) is considered.⁷ The model studies only the region between the anode plane and the target. In experiments described in Ref. 7, the electron beam is injected into the drift tube through the hollow anode. In the model, the entrance into the drift tube, i.e., the anode, was simulated as a grounded foil through each the injection of electrons was considered. The model studies the processes of interaction between the rigid electron beam and Al atoms evaporated from the Al target (see Fig. 1), i.e., the processes that occur when the material of the target in the vicinity of its surface has already experienced phase transitions, and transfers to a highly heated liquid phase and starts to evaporate. In order to simulate the plasma formation and evolution, a 1D PIC code for planar geometry was developed. The surface area of the target and anode, both having zero potential, was considered to be 1 cm². The target–anode (T-A) gap was varied depending on the initial conditions.

The following sequence of steps was performed for each time step:

1. Injection of electrons from the anode with a constant energy of 100 keV.
2. Particle weighting on a spatial numerical grid. Two different grids were introduced, one for charged particles (electrons and ions) and one for neutrals. The grid for neutrals had a smaller step, $\Delta x = 5 \times 10^{-5}$ cm, than that for charged particles (electrons and ions), $\Delta x = 2 \times 10^{-2}$ cm, in order to describe precisely the neutrals' density and the electron-neutral interactions.
3. Solution of the Poisson equation for new electron and ion densities.⁸
4. Propagation of electrons, ions, and neutrals into new positions.⁸ The relativistic motion equations were solved for electrons. When the new position and velocity of an

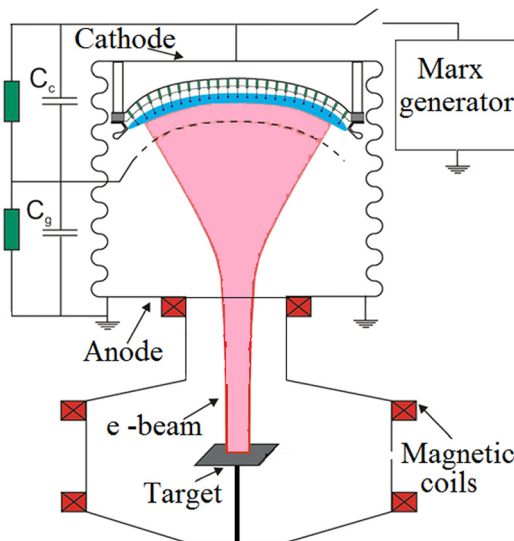


FIG. 1. Schematic of the experimental setup of the GESA facility (see Ref. 7).

electron were defined, the possibility of this electron colliding with a neutral was evaluated. The ions which reach the anode foil were removed from the simulations.

5. Secondary electron emission (SEE) from the target occurred when beam electrons reached the target. The process of SEE develops continuously in time, which cannot be described in discrete PIC models. Therefore, the initial position of secondary electrons was randomly distributed in interval $0 < x \leq 10^{-5}$ cm and the initial velocity in the interval $0 < v_e \leq 10^7$ cm/s.
6. Injection of neutrals evaporated from the target. All neutrals had a constant velocity of 2×10^5 cm/s. The rate of evaporation was equal to 10^{24} particle/(cm²·s).⁷ Such values of the neutrals' velocity and evaporation rate provide an almost constant density ($n_n \sim 10^{19}$ cm⁻³) of neutrals in the vicinity of the target;
7. The reflection of high-energy beam electrons from the target with a reflection coefficient of 0.17 and electron energy distribution was taken into account following the data presented in Ref. 9.
8. Elastic reflection of electrons from the anode.
9. Return to Step 1.

Three types of collisions between electrons and neutrals were considered, namely, impact ionization, elastic scattering, and excitation of the first electronic energy level. The ionization cross section of the Al neutral atom, which is valid for electron energy¹⁰ $\varepsilon_e \leq 10$ keV, was extrapolated for the high-energy electrons as¹¹

$$\sigma_{ion} = \frac{C}{\varepsilon_e \varepsilon_{ion}} \ln(\varepsilon_e / \varepsilon_{ion}),$$

where $C = 14.4 \times 10^{-14}$ cm²·eV², and $\varepsilon_{ion} \approx 6$ eV is the ionization energy of the Al atom. The probability of an electron–atom collision was defined as¹²

$$P = 1 - \exp[-\Delta r / \lambda(\varepsilon_e)],$$

where Δr is the distance that electrons propagate during one time step and $\lambda(\varepsilon_e)$ is the mean free path of electrons,

$$\lambda(\varepsilon_e) = \frac{1}{N \times [\sigma_{el}(\varepsilon_e) + \sigma_{ion}(\varepsilon_e) + \sigma_{ex}(\varepsilon_e)]}.$$

The probability of a collision was compared with the random number, rnd, in interval (0;1). If the value $\text{rnd} < P$, then an electron collision occurs, and another random number was generated in order to define the type of collision. In addition, the electron forward and backward scattering in both the elastic and inelastic processes was considered. The direction of the electron propagation after the collision was defined¹⁴ by the sign of $\cos \left[1 - \frac{2 \cdot \text{rnd}^*}{1 + 8 \cdot \varepsilon_n \cdot (1 - \text{rnd}) / \varepsilon_0} \right]$, where rnd* is the other random number, ε_n is the energy of the electron after the collision, and $\varepsilon_0 = 27.21$ eV is the atomic unit of energy. If the sign of cos is positive, the electrons do not change the direction of propagation. Otherwise, the electrons start to propagate in the opposite direction.

In each process of neutral atom ionization, one electron-ion pair was generated. The newly generated electron is

added to the primary electrons. The energy of these electrons was defined as¹¹

$$\varepsilon_{\text{eject}} = \varepsilon_1 \cdot \tan\{\text{rnd} \cdot \arctan[0.5 \cdot (\varepsilon_e - \varepsilon_{\text{ion}})/\varepsilon_1]\},$$

where ε_1 is the function that fits the experimental data; it is known for several gases,¹³ and according to Ref. 12, it is constant and equal to ~ 10 eV. It was supposed that these newly generated electrons propagate forward or backward with equal probability. Therefore, the angle $\alpha = 2\pi \cdot \text{rnd}$ (rnd is another random number) was calculated and the direction of the propagation of the electron was defined by the sign of $\cos(\alpha)$. The initial ion's velocity was assumed to be equal to the velocity of a neutral atom, i.e., 2×10^5 cm/s. The location of the generated electron-ion pair was determined by the coordinate of the primary ionizing electron.

If the current density of the electron beam is large enough, it is obtained that a virtual cathode (VC) is formed by the space charge of the beam in the T-A gap. It is understood that 1D simulations cannot be applied to obtain an actual potential distribution in the T-A gap. Therefore, three-dimensional PIC simulations that considered the propagation of the electron beam in a vacuum tube of physical geometry (see Fig. 1) were carried out using KARAT software¹⁵ in order to check the possibility of a VC forming for the given parameters (energy of the beam electrons ε_b and electron current density j_b) of the magnetized rigid electron beam. An example of the results of these simulations at time delay $\tau_d = 50$ ns with respect to the beginning of the electron beam injection from the anode plane ($z=0$) with $\varepsilon_b = 100$ keV and $j_b = 10$ A/cm², when one obtains a steady state potential distribution, is shown in Fig. 2.

One can see that, with these electron beam parameters, VC formation occurs. In addition, the results of these simulations showed that there is no VC formation when the electron

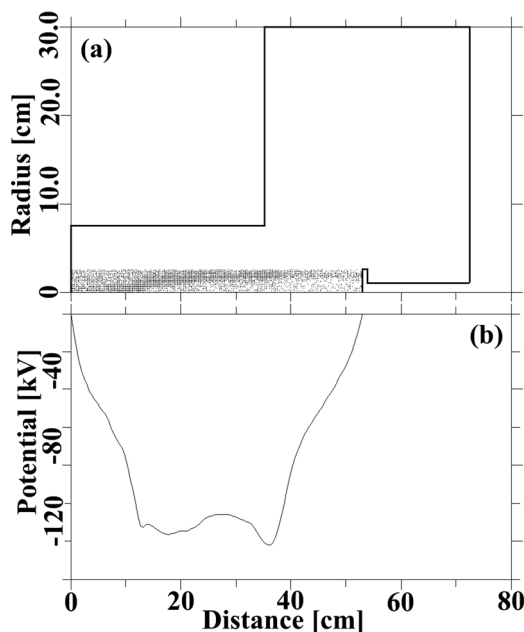


FIG. 2. The results of 3D PIC simulations for physical experimental geometry (see Fig. 1) for beam parameters $\varepsilon_b = 100$ keV and $j_b = 10$ A/cm² at $\tau_d = 50$ ns.

beam parameters are $j_b = 5$ A/cm² and $\varepsilon_b = 100$ keV. In the case of 1D simulations, a qualitatively similar potential distribution with the formation of the VC was obtained for $d_{TA} = 7$ cm, i.e., at this value of d_{TA} the depth of the potential well was almost equal to the depth of the potential well obtained in 3D simulations for the same parameters of the electron beam.

III. RESULTS AND DISCUSSION

1D PIC numerical simulations were carried out for electron beams with $\varepsilon_b = 50, 100,$ and 200 keV and current density $j_b = 5, 10,$ and 15 A/cm², and $d_{TA} = 7$ cm, which resulted in VC formation, and for $j_b = 5$ A/cm² and $\varepsilon_b = 100$ keV simulations were carried out for $d_{TA} = 9$ cm, which is the upper limit of the value of the TA gap when there is no VC formation. The distributions of the potential for $j_b = 10$ A/cm² and $\varepsilon_b = 100$ keV at different values of τ_d are shown in Figs. 3(a) and 3(b). One can see that the VC is formed near the anode. Later, when ions emitted from the target's plasma boundary are accelerated toward the anode, the VC shifts toward the anode and its absolute maximal potential oscillates around 100 kV [see Fig. 4(a)].

In the simulations, it was considered that the density of evaporated neutrals is $\sim 10^{19}$ cm⁻³, which corresponds to neutrals flow of 10^{24} particles/(s·cm²) and a velocity of 2×10^5 cm/s. The mean free path for electrons with $\varepsilon_e = 100$ keV can be estimated as $\lambda_e = (n_n \sigma)^{-1} \approx 0.04$ cm for $\sigma \approx 2.5 \times 10^{-18}$ cm². Thus, it can be expected that intense vapor ionization by the electron beam would begin at $\tau_d \geq 0.2$ μ s, when neutrals fill the volume in the vicinity of the target having a length of ~ 0.04 cm. However, one can see in Fig. 3(a) that the potential distribution already starts to be disturbed at $\tau_d \sim 0.06$ μ s. The latter occurs since the electrons that are reflected from the target have a smaller energy than that of the beam electrons. Consequently, the mean free path of the reflected electrons is smaller and ionization starts earlier than it would start these reflected electrons were not taken into account. It is important to note that the secondary

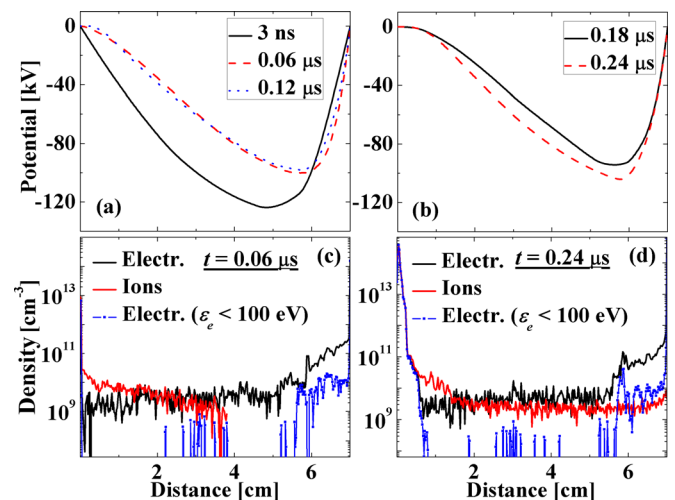


FIG. 3. (a,b) Potential distribution and (c,d) distribution of electrons (with all energies and with the energies smaller than 100 eV) and ions at different times. $j_b = 10$ A/cm², $\varepsilon_b = 100$ keV.

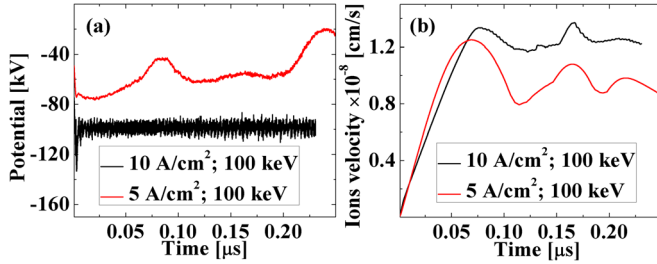


FIG. 4. (a) Time dependence of the potential well depth (a) and largest ion velocity (b) in the T-A gap at $j_b = 10 \text{ A/cm}^2$ and $\varepsilon_b = 100 \text{ keV}$ and $j_b = 5 \text{ A/cm}^2$ and $\varepsilon_b = 100 \text{ keV}$.

emitted electrons cannot ionize the gas because the energy of these electrons is smaller than the value of ε_{ion} for Al atoms. In addition, these electrons are emitted into the space where the time-dependent potential has either a negative slope [see Fig. 3(a)] or is smaller than ε_{ion}/e .

Figs. 3(c) and 3(d) show the distribution of the density of electrons with all energies and with $\varepsilon_e < 100 \text{ eV}$ (the latter will be considered as “plasma” electrons) and ions at $\tau_d = 0.06 \mu\text{s}$ and $\tau_d = 0.24 \mu\text{s}$. One can see fast ion propagation toward the anode, which leads to partial neutralization of the electron beam space charge and, respectively, to a decrease in the depth of the potential well and its shift toward the anode [see Fig. 3(b)]. The simulation results showed also the formation of a low-ionized plasma with density $\leq 4 \times 10^{14} \text{ cm}^{-3}$ in the vicinity of the target. The density of the plasma obtained in the present simulations agrees rather well with the data of spectroscopic measurements presented in Ref. 7. This plasma acquires the target potential and propagates toward the anode at a velocity, V_f , significantly smaller than that of the energetic ions, V_i . The value of V_f was defined by the shift toward the anode of the plasma, which acquires a potential almost equal to that of the target. For the case $j_b = 10 \text{ A/cm}^2$ and $\varepsilon_b = 100 \text{ keV}$, the plasma expansion velocity is $V_f \approx 1.2 \times 10^4 \text{ m/s}$, while the maximum value of V_i is $\sim 1.38 \times 10^6 \text{ m/s}$. Table I presents a comparison of some parameters of the plasma generated at different values of j_b and ε_b . One can see that the increase in the current density j_b for constant ε_b leads to an increase in the density of the plasma and the velocity of the plasma front propagation. In the case of an increase in the electron energy ε_b , while j_b remains constant, one obtains only a slight change in the plasma density and increase in the plasma front propagation V_f .

The simulation results showed that the energy of ions accelerating toward the anode is influenced by the formation

TABLE I. Influence of the electron beam energy and current density on the plasma density, velocity of the plasma front propagation, and the ions’ velocity.

Beam parameters	$n_e^{\text{max}}, 10^{14} \text{ cm}^{-3}$	$V_f, 10^6 \text{ cm/s}$	$V_i^{\text{max}}, 10^8 \text{ cm/s}$
100 keV; 5 A/cm ²	0.69	0.90	1.25
100 keV; 10 A/cm ²	3.60	1.24	1.38
100 keV; 15 A/cm ²	4.12	3.40	1.34
200 keV; 10 A/cm ²	1.38	5.50	1.73
50 keV; 10 A/cm ²	3.38	0.98	1.00

of the VC. Fig. 4 shows a comparison of the results obtained for two electron beam parameters, $j_b = 10 \text{ A/cm}^2$ and $\varepsilon_b = 100 \text{ keV}$, when a VC is formed, and for $j_b = 5 \text{ A/cm}^2$ and $\varepsilon_b = 100 \text{ keV}$ when there is no VC formation. One can see that when a VC is formed, its potential oscillates near $\varphi \approx -100 \text{ kV}$ with the amplitude of the oscillations being $\pm 10 \text{ kV}$. When a VC is not formed, the depth of the potential well decreases in time. The difference in the behavior of potential distribution leads to the ion velocity having a different time dependence [see Fig. 4(b)], which is almost constant when a VC forms and decreases in time when a VC is not formed. In the latter case, the maximal velocity of ions increases up to $V_i \sim 1.38 \times 10^6 \text{ m/s}$ and then decreases. The increase in the value of V_i is caused by the acceleration of ions in the potential well formed by a non-compensated electron beam. When the space charge of the electron beam starts to be compensated by ions, the depth of the potential well decreases and the ions’ velocity decreases. These energetic ions, the current density of which reaches $j_i = 0.35 \text{ A/cm}^2$, could change significantly the parameters of the electron diode generating electron beam. Indeed, penetration of these ions through the anode into the anode-cathode gap will cause partial compensation of the space charge of the electron beam, thus leading to an increase in the space-charge limited current density. In addition, interaction of these energetic ions with the cathode could lead to its erosion, thus decreasing its life-time, and to the formation of additional dense plasma on the cathode surface. The expansion of this plasma toward the anode could lead to a local increase in the emitted local current density and to non-uniform current density cross-sectional distribution, as well as to shorting of the anode-cathode gap.

The electron energy distribution function (EEDF) $f(\varepsilon)$ of the plasma electrons at a distance of 0.1 cm from the target at values of τ_d is shown in Fig. 5. One can see that there is a significant high-energy tail in the EEDF, which allows one to conclude that this distribution is non-Maxwellian. In addition, one can see that the EEDF changes in time. The average electron energy, which was defined as

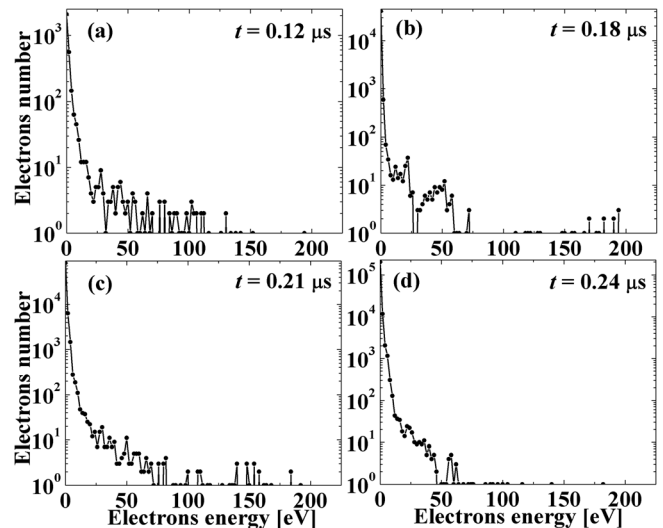


FIG. 5. Electron energy distribution function at the distance of 10^{-3} m from the cathode at different values of τ_d . $j_b = 10 \text{ A/cm}^2$, $\varepsilon_b = 100 \text{ keV}$.

$$\bar{\varepsilon} = \frac{\int f(\varepsilon) \cdot \varepsilon \cdot d\varepsilon}{\int f(\varepsilon) \cdot d\varepsilon},$$

gives ~ 0.7 eV, which is in good agreement with the experimental results presented in Ref. 7.

In addition, the influence of the SEE from the target on the plasma parameters was studied. Two models were considered, namely, a model that does and one that does not consider the SEE. The coefficient of the SEE was constant¹⁶ and equal to 0.6. The energy of these emitted electrons does not exceed the ionization potential of *Al*. Therefore, secondary emitted electrons do not ionize gas and they experience only elastic collisions. However, injection of these secondary electrons into the plasma leads to a decrease in the plasma density (see Fig. 6) and to an increase in the plasma expansion velocity. The results of simulations showed $V_f \approx 2.5 \times 10^6$ cm/s in the model that considers the SEE and $V_f \approx 2 \times 10^6$ cm/s in the model that does not. In addition, without SEE, the results of simulation results showed an increase in ion current density through the anode. Namely, $j_i = 0.51$ A/cm² and $j_i = 0.35$ A/cm² in the cases without and with SEE, respectively. These results can be explained by the enhanced ambipolar diffusion of the plasma caused by the injection of secondary electrons.

Using the average energy of electrons and density of plasma n_e in the vicinity of the cathode, one can estimate the conductivity of the generated plasma using the expression for the conductivity of a rather cold low-ionized plasma,¹⁷

$$\sigma = \frac{e^2 n_e}{m_e \cdot \bar{V}_e \cdot n_g \cdot \sigma_m} \approx 0.3 \Omega^{-1} \text{cm}^{-1}$$

where m_e is the electron mass, $n_e = 3.6 \times 10^{14}$ cm⁻³ is the electron density, \bar{V}_e is the average electron velocity corresponding to the energy of electrons $\varepsilon_e \approx 0.7$ eV, $n_g = 10^{19}$ cm⁻³ is the density of the evaporated vapors, and $\sigma_m = 9 \times 10^{-16}$ cm² is the cross-section for momentum transfer for electrons with $\varepsilon_e \approx 0.7$ eV. The value of the conductivity that is obtained is rather small, which for the considered values of j_b results in only a few kV potential difference along a plasma channel a few cm in length.

The formation and expansion of this low-ionized plasma can be considered as a natural limit for the duration of the high-voltage phase during which one generates a high-energy

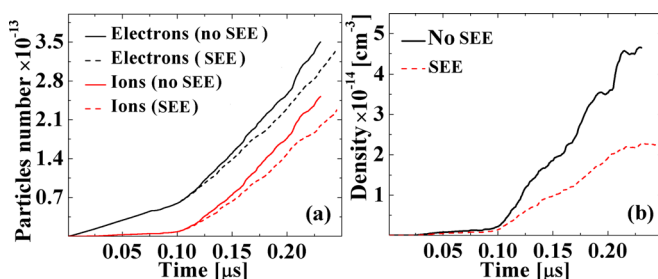


FIG. 6. (a) Time dependence of the electron and ion numbers inside the T-A gap and (b) time dependence of the plasma density in the models that do and do not consider the SEE from the target. $j_b = 10$ A/cm², $\varepsilon_b = 100$ keV.

electron beam. In the present research, only a few μ s of the plasma evolution were considered because the simulation time was limited. Therefore, we do not have data concerning the axial distribution of the plasma density for different times. In addition, the present numerical simulations do not consider the decrease in the neutral density versus the distance from the cathode. It is understood that considering this effect, one would obtain a decrease in the plasma density versus the distance from the target. Nevertheless, one can consider the situation when this plasma, even with a significantly decreased density ($\sim 10^{11}$ cm⁻³), penetrates the anode, placed at a distance of 40 cm from the target, leading to shorting of the anode-cathode gap within $(1-2) \times 10^{-4}$ s, and respectively, to the termination of the high-voltage phase. Qualitatively, this phenomenon was described in Ref. 7 as the simultaneous appearance of intense light emission at different distances from the target, which coincides with termination of the accelerating voltage at typical values of $\tau_d \geq 140$ μ s.

IV. SUMMARY

Numerical simulations of the dynamics of the plasma generated during the interaction of high-energy and high-current electron beams with *Al* vapors were carried out using 1D PIC code. The results of these simulations showed that the generated plasma is low-ionized and characterized by non-Maxwellian electron energy distribution. The density and electron temperature of the plasma does not exceed 4×10^{14} cm⁻³ and 1 eV, respectively, for the parameters of the electron beam current density and energy, which were considered in good agreement with the experimental results presented in Ref. 7. This target's plasma propagates toward the anode at a typical velocity of $\sim 10^6$ cm/s. In addition, the simulation results showed that the ions are accelerated from the plasma front toward the anode by the potential of the non-compensated space charge of the electron beam. The typical velocity of these energetic ions is $\sim 10^8$ cm/s and depends on the electron current density and energy. These ions partially compensate the space charge of the electron beam, which leads to a decrease in the depth of the potential well and can change significantly the parameters of the electron diode when ions penetrate the anode and pass into the interelectrode space.

ACKNOWLEDGMENTS

This work was supported in part at the Technion by a fellowship from the Lady Davis Foundation.

- ¹D. I. Proskurovsky, V. P. Rotshtein, G. E. Ozur, Yu. F. Ivanov, and A. B. Markov, *Surf. Coat. Technol.* **125**, 49 (2000).
- ²G. Mueller, G. Schumacher, and D. Strauss, *Surf. Coat. Technol.* **108**, 43 (1998).
- ³T. J. Renk, P. P. Provencio, S. V. Prasad, A. S. Shlapakovski, A. V. Petrov, K. Yatsui, W. Jiang, and H. Suematsu, *Proc. IEEE* **92**, 1057 (2004).
- ⁴V. Engelko, B. Yatsenko, G. Mueller, and H. Bluhm, *Vacuum* **62**, 211 (2001).
- ⁵G. Mueller, V. Engelko, A. Weisenburger, and A. Heinzel, *Vacuum* **77**, 469 (2005).
- ⁶V. Engelko and G. Mueller, *J. Appl. Phys.* **98**, 013303 (2005).

- ⁷W. An, Ya. E. Krasik, R. Fetzer, B. Bazylev, G. Mueller, A. Weisenburger, and V. Bernshtam, *J. Appl. Phys.* **110**, 093304 (2011).
- ⁸C. K. Birdsall and A. B. Langdon, *Plasma Physics via Computer Simulation* (IoP Publishing, Bristol, 1991).
- ⁹V. Engelko, V. Kuznetsov, G. Viazmenova, G. Mueller, and H. Bluhm, *J. Appl. Phys.* **88**, 3879 (2000).
- ¹⁰See <http://physics.nist.gov/cgi-bin/Ionization/atom.php?element=Al> for electron impact ionization cross section of Al atoms.
- ¹¹Y.-K. Kim, *J. Res. Natl. Inst. Stand. Technol.* **97**, 689 (1992).
- ¹²V. Vahedi and M. Surendra, *Comput. Phys. Commun.* **87**, 179 (1995).
- ¹³C. B. Opal, W. K. Peterson, and E. C. Beaty, *J. Chem. Phys.* **55**, 4100 (1971).
- ¹⁴A. Okhrimovskyy, A. Bogaerts, and R. Gijbels, *Phys. Rev. E* **65**, 037402 (2002).
- ¹⁵V. P. Tarakanov, User's Manual for Code KARAT, ver.7.09, April, 1999.
- ¹⁶I. K. Kikoin, *Tables of Physical Quantities* (Atomizdat, Moscow, 1976) (in Russian).
- ¹⁷M. A. Lieberman and A. J. Lichtenberg, *Principles of Plasma Discharges and Materials Processing* (John Wiley and Sons, New York, 1994).